Methods for controlling voltage and power to achieve high efficiency inductive charging under variable operating conditions

Giuseppe Guidi [1] **Jon Are Suul** [1),2)]

1) SINTEF Energy, Trondheim, Norway

E-mail: giuseppe.guidi@sintef.no

Jon.A.Suul@sintef.no

2) Norwegian University of Science and Technology (NTNU), Trondheim, Norway

ABSTRACT: This paper discusses the problem of controlling the power flow in inductive charging systems under variable operating conditions when the only degree of freedom is the modulation of the primary-side converter. Operating conditions are dictated by coupling and by the dc voltages on either side of the system. When operating conditions are deviating from the rated values and frequency cannot be changed, voltage regulation is needed to keep the power flow at the required level without exceeding any of the system maximum limits. Several methods are analyzed and compared, with the aim of finding the best strategy to achieve precise and safe power regulation without incurring excessive losses, both in the coils and in the power converters. It is shown that it is key for maintaining high efficiency to avoid switching of high currents, which happens when adopting phase-shift modulation. Pulse-skipping techniques limit the switching losses but may give rise to low-frequency oscillations. This aspect is analyzed and a modified Delta-Sigma Modulation algorithm for pulse-skipping pattern generation is presented, which prevents the appearance of limit cycles that excite the poorly damped natural oscillation mode of the system.

KEY WORDS: Inductive power transfer, Oscillations, Pulse skipping modulation, Wireless charging systems

1. INTRODUCTION

Inductive Power Transfer (IPT) technology is being increasingly utilized in a diverse range of applications, especially for battery charging of electric vehicles (EVs)[(1)], autonomous underwater vehicles[(2)] and marine vessels[(3)]. In high-power IPT systems, the primary design objectives include low cost, simplicity and reliability, high power density, and high efficiency. For applications intended to operate with significant variations in load and coupling coefficient, one of the main challenges of system-level design is to maintain high efficiency across the full range of operating conditions

The series-series (SS) compensated ITP topology with a diode rectifier on the pickup side, as shown in Fig. 1, is often deemed the most suitable choice for high-power inductive battery charging applications from considerations on cost, complexity, and power density [(3)]. Since only the operating frequency and the primary-side AC voltage can be regulated, there are limited degrees of freedom in the control of such systems. This imposes challenges for the control design and makes it more difficult to achieve high efficiency over a wide range of operating conditions. However, it is possible to design the system in a way that allows for sub-resonant frequency operation while maintaining rated power transfer at close to unity power factor over a wide range of coupling conditions. This approach was first introduced in [(4)] and enables IPT system design for handling large coupling variations with minimized component ratings. The dynamic performance and efficiency characteristics that can be achieved are analyzed in [(5),(6)].

While design for sub-resonant frequency control is very effective in limiting switching losses at high power and high coupling, the resulting power regulation range has a coupling-dependent lower bound. Thus, operation with sending-side voltage control is required to extend the regulation range down to zero power. Indeed, a coordinated operation of sub-resonant frequency control and voltage control at the resonance frequency is necessary to enable controlled operation in the full range of power and coupling conditions, as discussed in [(7)].

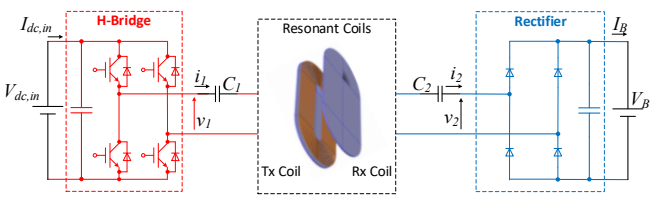

Fig. 1: SS-compensated inductive power transfer system.

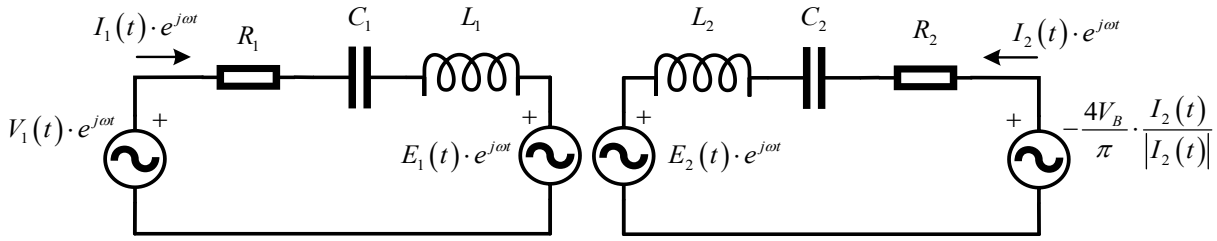

Fig. 2: Equivalent circuit of SS-compensated system with passive rectifier at secondary side.

Sending side voltage control for the topology in Fig. 1 can be achieved by either regulating the dc input voltage, $V_{dc,in}$, or by acting on the modulation of the H-bridge converter. However, control of the dc input voltage will typically require an additional DC-DC converter, which will increase losses, costs and complexity while reducing the power density. Thus, voltage control by the sending-side H-bride converter is preferred for high power systems.

When controlling the sending-side voltage in Fig. 1, it should also be considered that the Constant Voltage Load (CVL) characteristics introduced by the direct connection of a diode rectifier to the battery voltage, V_B, is causing a poorly damped oscillation when operating at the resonance frequency [8], [9]. Excitation of this oscillation mode can cause large over-currents in the system and will generate additional losses even if the average power transfer can be controlled. Thus, several strategies have been recently proposed for damping or preventing oscillations when applying sending-side voltage control to systems with CVL characteristics [9], [10], [11], [12].

This paper is first discussing the source of the poorly damped oscillations appearing in SS-compensated IPT systems with CVL characteristics when operating at the resonance frequency. Then, the main causes of losses arising under voltage control by the sending-side H-bridge converter are clarified and the general methods for power flow control that minimize the incurrence of such losses are outlined. Finally, an example of analysis of losses resulting from different types of voltage control methods are presented based on simulations with parameters from a prototype of a 100 kW IPT system.

2. DYNAMICS OF SS-COMPENSATED IPT SYSTEMS WITH CONSTANT VOLTAGE LOAD

2.1. Detailed dynamic model

The behavior of the SS-compensated system in Fig. 1 can be conveniently analyzed using first harmonic approximation (FHA) and dynamic phasors [8], [13], resulting in the equivalent system of Fig.2. Note that all voltages and currents in the figure are expressed in the generic complex phasor notation:

$$X(t) = X_{\mathrm{Re}}(t) + j \cdot X_{\mathrm{Im}}(t) \tag{1}$$

Dynamic phasors are used to describe the variation in time of the amplitude of the voltages/currents without focusing on the oscillations at fundamental frequency ω. The complex phasor equations of the system are written as **Error! Reference source not found.**:

$$\begin{cases} V_1(t) = R_1 I_1(t) + V_{L1}(t) + V_{C1}(t) + E_1(t) \\ -\frac{4V_B}{\pi}\cdot e^{j\cdot\angle I_2(t)} = R_2 I_2(t) + V_{L2}(t) + V_{C2}(t) + E_2(t) \\ C_1\cdot\frac{dV_{C1}}{dt} + j\omega C_1 V_{C1}(t) = I_1(t) \\ C_2\cdot\frac{dV_{C2}}{dt} + j\omega C_2 V_{C2}(t) = I_2(t) \\ V_{L1}(t) = L\cdot\frac{dI_1(t)}{dt} + j\omega L I_1(t) \\ V_{L2}(t) = L\cdot\frac{dI_2(t)}{dt} + j\omega L I_2(t) \\ E_1(t) = M\frac{dI_2(t)}{dt} + j\omega M I_2(t) \\ E_2(t) = M\frac{dI_1(t)}{dt} + j\omega M I_1(t) \end{cases} \tag{2}$$

The system is of 8th order and is non-linear, due to the relationship between the secondary current and voltage that describes the action of the passive rectifier [8]. Applying standard techniques for linearization and small-signal analysis, it can be verified that the system has a dominant oscillatory mode whose natural frequency of oscillation is dependent on system parameters and operating conditions. Knowledge of this mode is essential for control system design and is particularly important in case of voltage control with pulse-skipping techniques, as will be shown in a later section.

2.2. Simplified reduced-order model

To obtain a simple analytical expression for the dominant oscillatory mode, two key approximations can be made that correspond to neglecting high frequency components. Firstly, the back-emf terms are simplified by assuming a zero-order transfer function between the phasors:

$$\begin{cases} \frac{E_1(s)}{I_2(s)} = sMI_2(s) + j\omega MI_2(s) \approx j\omega MI_2(s) \\ \frac{E_2(s)}{I_1(s)} = sMI_1(s) + j\omega MI_1(s) \approx j\omega MI_1(s) \end{cases} \tag{3}$$

Additionally, the LC series connection is treated as a single component and the order of the transfer function between the voltage and current phasors is reduced from two to one by applying Taylor approximation around s=0 [15]. This results in:

$$\begin{aligned}\frac{V_{L,1(2)}(s)+V_{C,1(2)}(s)}{I_{1(2)}(s)} &= sL_{1(2)} + j\omega L_{1(2)} + \frac{1}{sC_{1(2)} + j\omega C_{1(2)}} \\ &\approx L_{1(2)}\frac{{\omega_{r,1(2)}}^2+\omega^2}{\omega^2}s + j\frac{\omega^2-{\omega_{r,1(2)}}^2}{\omega}L_{1(2)}\end{aligned} \tag{4}$$

with:

$$\omega_{r,1} = \frac{1}{\sqrt{L_1 \cdot C_1}}; \quad \omega_{r,2} = \frac{1}{\sqrt{L_2 \cdot C_2}} \tag{5}$$

As a result, the dynamic system model is reduced to a 4th order representation. Further simplification can be achieved by assuming a perfectly tuned system and operation at the resonant frequency:

$$\omega_{r,1} = \omega_{r,2} = \omega \tag{6}$$

Applying all the simplifications, while separating the real and imaginary parts of the phasors and aligning the real axis with the primary voltage phasor, leads to:

$$\begin{cases}\frac{dI_{1,\mathrm{Re}}(t)}{dt} = -\frac{R_1}{2L_1}\cdot I_{1,\mathrm{Re}}(t) + \frac{\omega M}{2L_1}\cdot I_{2,\mathrm{Im}}(t) + \frac{1}{2L_1}\cdot V_1(t) \\ \frac{dI_{1,\mathrm{Im}}(t)}{dt} = -\frac{R_1}{2L_1}\cdot I_{1,\mathrm{Im}}(t) - \frac{\omega M}{2L_1}\cdot I_{2,\mathrm{Re}}(t) \\ \frac{dI_{2,\mathrm{Re}}(t)}{dt} = -\frac{R_2}{2L_2}\cdot I_{2,\mathrm{Re}}(t) + \frac{\omega M}{2L_2}\cdot I_{1,\mathrm{Im}}(t) + \frac{1}{2L_2}\cdot V_{2,\mathrm{Re}}(t) \\ \frac{dI_{2,\mathrm{Im}}(t)}{dt} = -\frac{R_2}{2L_2}\cdot I_{2,\mathrm{Im}}(t) - \frac{\omega M}{2L_2}\cdot I_{1,\mathrm{Re}}(t) + \frac{1}{2L_2}\cdot V_{2,\mathrm{Im}}(t) \\ V_{2,\mathrm{Re}}(t) = -\frac{4V_B}{\pi}\cdot\frac{I_{2,\mathrm{Re}}(t)}{|I_2(t)|} \\ V_{2,\mathrm{Im}}(t) = -\frac{4V_B}{\pi}\cdot\frac{I_{2,\mathrm{Im}}(t)}{|I_2(t)|}\end{cases} \tag{7}$$

This reduced order system can then be linearized around a stable operating point. For operation at resonance, steady-state operation is characterized by:

$$\bar{I}_1 = \bar{I}_{1,\mathrm{Re}}; \quad \bar{I}_2 = j\cdot\bar{I}_{2,\mathrm{Im}} \tag{8}$$

The linearized, 4th order system can then be expressed as:

$$\frac{d}{dt}\begin{bmatrix}\Delta I_{1,\mathrm{Re}}\\ \Delta I_{1,\mathrm{Im}}\\ \Delta I_{2,\mathrm{Re}}\\ \Delta I_{2,\mathrm{Im}}\end{bmatrix} = \begin{bmatrix}\frac{-R_1}{2L_1} & 0 & 0 & \frac{\omega M}{2L_1}\\ 0 & \frac{-R_1}{2L_1} & \frac{-\omega M}{2L_1} & 0\\ 0 & \frac{\omega M}{2L_2} & \left(\frac{-R_2}{2L_2}+\frac{-2V_B}{\pi L_2 \bar{I}_{2,\mathrm{Im}}}\right) & 0\\ \frac{-\omega M}{2L_2} & 0 & 0 & \frac{-R_2}{2L_2}\end{bmatrix}\begin{bmatrix}\Delta I_{1,\mathrm{Re}}\\ \Delta I_{1,\mathrm{Im}}\\ \Delta I_{2,\mathrm{Re}}\\ \Delta I_{2,\mathrm{Im}}\end{bmatrix} + \begin{bmatrix}\frac{1}{2L_1} & 0 & 0 & 0\end{bmatrix}^T\cdot\Delta V_1 \tag{9}$$

The state-space model in (9) describes two decoupled 2nd order systems, with the system consisting of the second and third equations being stable and without forcing terms. Thus, the complete system dynamics are expressed by the second-order system describing the evolution of the real part of the primary current phasor and the imaginary part of the secondary current phasor:

$$\frac{d}{dt}\begin{bmatrix}\Delta I_{1,\mathrm{Re}}\\ \Delta I_{2,\mathrm{Im}}\end{bmatrix} = \begin{bmatrix}-\frac{R_1}{2L_1} & \frac{\omega M}{2L_1}\\ -\frac{\omega M}{2L_2} & -\frac{R_2}{2L_2}\end{bmatrix}\cdot\begin{bmatrix}\Delta I_{1,\mathrm{Re}}\\ \Delta I_{2,\mathrm{Im}}\end{bmatrix} + \begin{bmatrix}\frac{1}{2L_1}\\ 0\end{bmatrix}\cdot\Delta V_1 \tag{10}$$

Since losses associated to R_1, R_2 are very small by design, this system has a very poorly damped oscillatory mode with natural frequency given by:

$$\omega_n \approx \frac{\omega M}{2\sqrt{L_1 \cdot L_2}} = \frac{\omega \cdot k}{2} \tag{11}$$

This expression is identical to the result obtained with a different approach for model order reduction in [16], and shows explicitly how the natural oscillation frequency is directly linked to the coupling coefficient k.

3. EFFICIENCY AND LOSSES OF IPT SYSTEMS

The power transfer efficiency in inductively coupled systems has an upper bound that is independent of the compensation strategy and is only related to the coupling coefficient k and the unloaded quality factor of the coils Q_1, Q_2 [4], [17]:

$$\eta_{\max} = \frac{k^2 Q_1 Q_2}{\left(1+\sqrt{1+k^2 Q_1 Q_2}\right)^2} \tag{12}$$

Unfortunately, maximum efficiency can only be achieved at a single operating point, where the receiving-side voltage and current satisfy the ideal load matching condition:

$$\left(\frac{V_B}{I_B}\right)_{matched} = \frac{\pi^2}{8}\cdot R_2 \cdot \sqrt{1+k^2 Q_1 Q_2} \tag{13}$$

In all other conditions, that inevitably present themselves when the battery voltage and current change during the charging process and/or when the coupling change due to relative coil movement, the efficiency will be lower. As mentioned, the system in Fig.1 gives only two degrees of freedom for controlling the power flow (i.e. the charging current) under non-nominal conditions: i.e. operating frequency ω and equivalent primary voltage V_1.

Primary voltage regulation negatively affects efficiency in several ways. For a given power flow, the current I_1 increases when V_1 decreases (as the power factor remains close to unity if operating at resonance), thus causing more conduction losses both in the coils and in the converter switches. Moreover, the switching

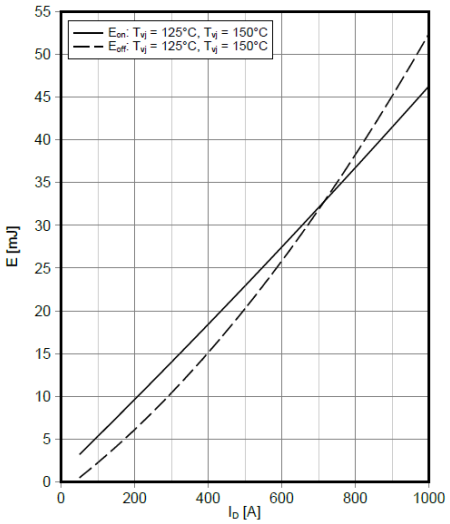

Fig. 3: Switching energy of 1200V, 500A SiC MOSFET (taken from datasheet[19]).

patterns used for voltage regulation may cause an increase in losses as the commutations of the solid-state devices may take place when the current in the switches is no longer close to zero [5]. Hard turn-on (loss of ZVS) can also appear, introducing potential EMI issues besides the increase of losses.

The increase in turn-off losses despite operation with ZVS is often underestimated but proves to be a major contributor to loss of efficiency in high power IPT systems designed to operate at high frequency. As a numerical example, Fig. 3 shows the switching energy of the SiC MOSFET device used in the 100kW, 80 kHz IPT prototype described in [18]. The system features 97% dc-dc efficiency when operated under nominal conditions, with a primary coil current of about 165 A_{RMS}. If the system is driven out of resonance and the H-bridge is forced to operate in ZVS with turn-off current in the order of 150A, the best-case losses, calculated from ideal datasheet information, will amount to approximately 1.6% of the rated power. That corresponds to a 50% increase in total losses compared to rated conditions and, more importantly, to a 300% increase in losses in the H-bridge.

In the following sections, methods for power flow control which do not cause excessive switching losses in the converter are discussed.

4. VOLTAGE CONTROL WITH MINIMUM SWITCHING LOSS

With reference to Fig.1, switching losses can be minimized by commutating the H-bridge devices only when the current crosses zero (ideal ZVS). To achieve this with control of the H-bridge output voltage, while at the same time regulating the magnitude of the fundamental component of the primary voltage is only possible by applying pulse-skipping techniques. An example of H-bridge

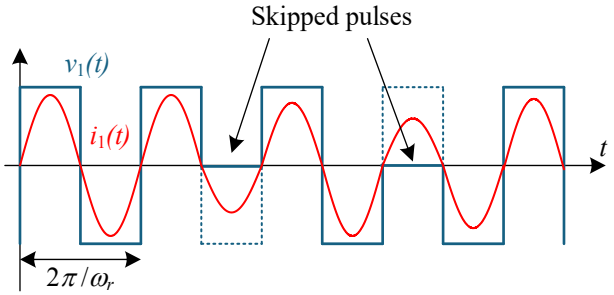

Fig. 4: Example of pulse-skipping voltage pattern.

output voltage generation with pulse-skipping is shown in Fig.4. The underlying idea is to suppress (skip) some of the half-periods of the square wave voltage at the resonant frequency, so that the long-term average of the fundamental component of the voltage applied at the primary side of the resonant coils can be controlled over the range:

$$0 \le V_{1,avg} \le \frac{4 \cdot V_{dc,in}}{\pi} \tag{14}$$

As long as the frequency of the underlying square wave is tuned to the resonant frequency of the SS-compensated system, all bridge commutations will happen when the current is ideally zero, as schematically shown in the figure, thus avoiding switching losses.

In the literature, many different methods for generating the pulse-skipping patterns have been proposed. On-Off keying modulation methods [20], [21] result in very low frequency subharmonics of the voltage pattern, causing the current to pulsate between zero and a maximum value that only depends on coupling and I/O dc voltages. Heavy filtering is thus needed to avoid severe pulsations in the charging power. Moreover, conduction losses due to the pulsating current pattern can be very high.

To reduce the current and power pulsations caused by pulse-skipping, the filtering action of the resonant coils themselves can be exploited by generating a voltage pattern that does not contain subharmonics at very low frequency. Some of the methods used for this purpose include fixed, pre-calculated pulse density modulation (PDM) patterns [22] , variable patterns generated using hysteresis control [11], [23] or delta-sigma modulation (DSM) techniques [9]. Model Predictive Control (MPC) has also been proposed for pattern generation [12]. These methods work satisfactorily in most operating conditions but may result in severe oscillations in some operating points. Oscillations appearing in the currents and power flow are then linked to the presence of subharmonics in the voltage pattern which correspond to the undamped natural modes of the system described in section 2.

Table 1 Main parameters of simulated IPT system

Rated power	$P_n = 100\,kW$
Rated I/O voltages	$V_{dc,in} = 700\,V$ $V_B = 700\,V$
Self-inductances	$L_1 = 37.9\,\mu H$ $L_2 = 36.7\,\mu H$
Resonant capacitances	$C_1 = C_2 = 110\,nF$
Operating frequency	$f = 80\,kH_z$
Rated coupling	$k_n = 0.207$

(a) – PSM-based voltage pattern generation

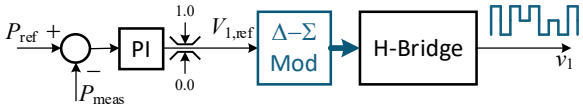

(b) – Voltage pattern generated by Δ–Σ modulator

Fig. 5: Schematic view of simulated control systems.

Generating a voltage pattern that minimizes current oscillations and always avoids resonances is not straightforward. One difficulty comes from the fact that the natural frequency of the system is a function of the coupling factor, as given by (11), which is not necessarily known and may change during operation. Another problem is that using pre-calculated patterns that are long enough to prevent resonant subharmonics and can be made adaptive to account for coupling variations, may result in slow control dynamics.

In the following, the focus is on DSM-based pattern generation methods, showing the clear advantages in terms of switching losses compared to conventional linear voltage control based on phase shift modulation (PSM). The problem of limit cycles arising in closed loop control that resonate with natural modes of the system is also highlighted and the effectiveness of a modified algorithm for voltage pattern generation is shown.

4.1. Comparison of converter losses under voltage control

As an example, the 100 kW IPT system described in [18] is simulated. The system has the same structure as in Fig.1 and its main parameters are summarized in Table 1. The charging control system is based on a conventional PI power regulator that generates the voltage command for the H-bridge. The per-unit voltage command is then fed in one case to a conventional phase-shift modulation (PSM) method as shown in Fig.5 (a) and in other cases to a half-period DSM implementation as shown in Fig.5 (b).

When the system is operated at rated power, both modulators output the same ideal square-wave voltage pattern, resulting in very low losses and no current oscillation, due to the absence of subharmonics. Estimated conduction and switching losses, constituting the base case for comparison, are reported in the first row of Table 2. The situation changes when the charging power needs to be controlled to a lower value, as shown in the simulations of Fig.6. In this case, the power reference is set to 50 kW, ideally resulting in a primary voltage reference of about 0.5 p.u.. Using PSM results in hard turn-on for the H-bridge devices, as well as turn-off with very high currents, as shown in Fig. 6 (a). However, the currents are completely free of low frequency oscillations. Fig. 6 (b) shows the results when applying DSM-based pulse-skipping modulation. In this case hard turn-on is avoided and the only switching losses are due to turn-off events at rather low current, which is close to the ideal situation (see Fig. 3). The currents show a hint of a low frequency component, but its effect on conduction losses is negligible. Switching and conduction losses estimated for the two kinds of modulation are reported in the second and third row of Table 2, highlighting the clear advantage of the pulse-skipping method.

The main issue related to the DSM-based control appears when the voltage pattern contains a low frequency component that resonates with the natural mode of the system, which, according to (11) and the parameters in Table 1, corresponds to:

$$f_n = \frac{\omega_n}{2\pi} = \frac{f \cdot k}{2} \approx 8.3\,kHz \tag{15}$$

It can be verified that the conventional 1-bit DSM implementation will give rise to a limit cycle with a low frequency component related to the p.u. voltage reference by:

$$f_{LC} = f \cdot \left(1 - \left|\frac{V_{1,ref} - 0.5}{0.5}\right|\right) \tag{16}$$

Table 2 - Estimated converter losses associated to different methods for primary voltage control

Power reference [kW]	PSM		Conventional 1-bit Delta-Sigma		Modified, Conditional Delta-Sigma	
	$P_{loss,cond}$ [W]	$P_{loss,sw}$ [W]	$P_{loss,cond}$ [W]	$P_{loss,sw}$ [W]	$P_{loss,cond}$ [W]	$P_{loss,sw}$ [W]
100	160	26	160	26	160	26
50	160	2400	160	290	160	290
95	160	859	190 (520 peak)	250 (700 peak)	165 (230 peak)	90 (280 peak)

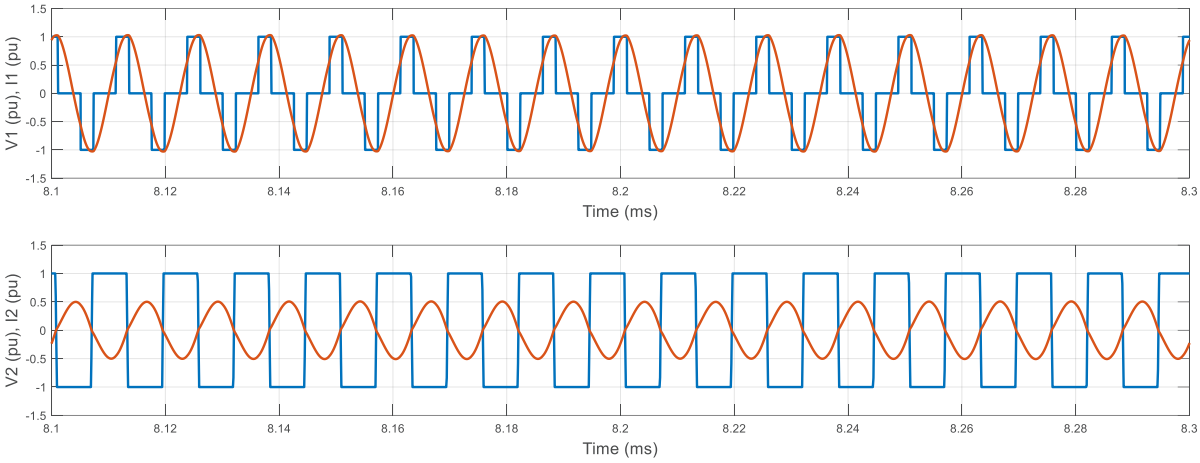

(a) – Phase-shift modulation

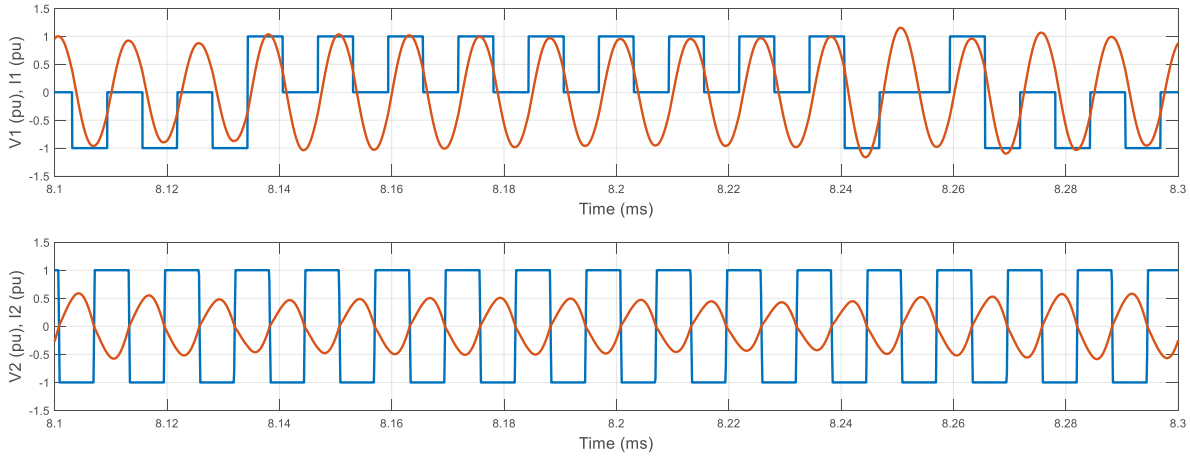

(b) – Pulse-skipping using Sigma-Delta modulation

Fig. 6: Simulated voltage and current waveforms of 100 kW IPT system. Power reference set to 50% of rated.

Resonance is therefore expected when:

$$f_{LC} = f_n \quad \Rightarrow \quad \begin{cases} \bar{V}_{1,ref,H} = 1 - \dfrac{k}{4} \approx 0.95 \\ \bar{V}_{1,ref,L} = \dfrac{k}{4} \approx 0.05 \end{cases} \tag{17}$$

The simulation in Fig. 8 (a) shows the behavior of the system with conventional DSM implementaiton when the power reference is set to 0.95 p.u., which corresponds approximately to the calculated resonant conditions. As expected, severe current oscillations at the natural frequency are observed, making operation inefficient and possibly impractical.

The problem can be mitigated by slightly modifying the DSM algorithm by adding additional conditions for pattern generation that account for the measured current, as first proposed in [10]. An implementation expanded from [10] is schematically shown in Fig. 7. The part in black in the figure is a conventional 1-bit Delta-Sigma modulator, while the part in red represents the proposed modification. The idea is to modify the conventional pattern by skipping extra-pulses when the measured current goes beyond a given threshold value I_{max} that can be calculated in advance. Moreover, a limit A_{max} is set for the DSM accumulator to avoid possible wind-up if the threshold is improperly set. It is noted that the modifications do not affect the long-term average of the output pattern, which is still guaranteed to correspond exactly to the per-unit reference. The ultimate result of the modifications is a

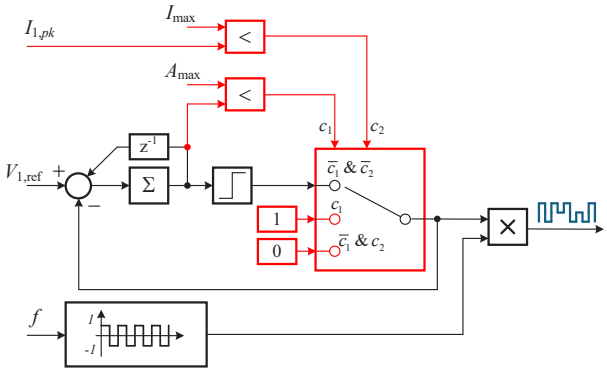

Fig. 7: Modified, Conditional Sigma-Delta modulator.

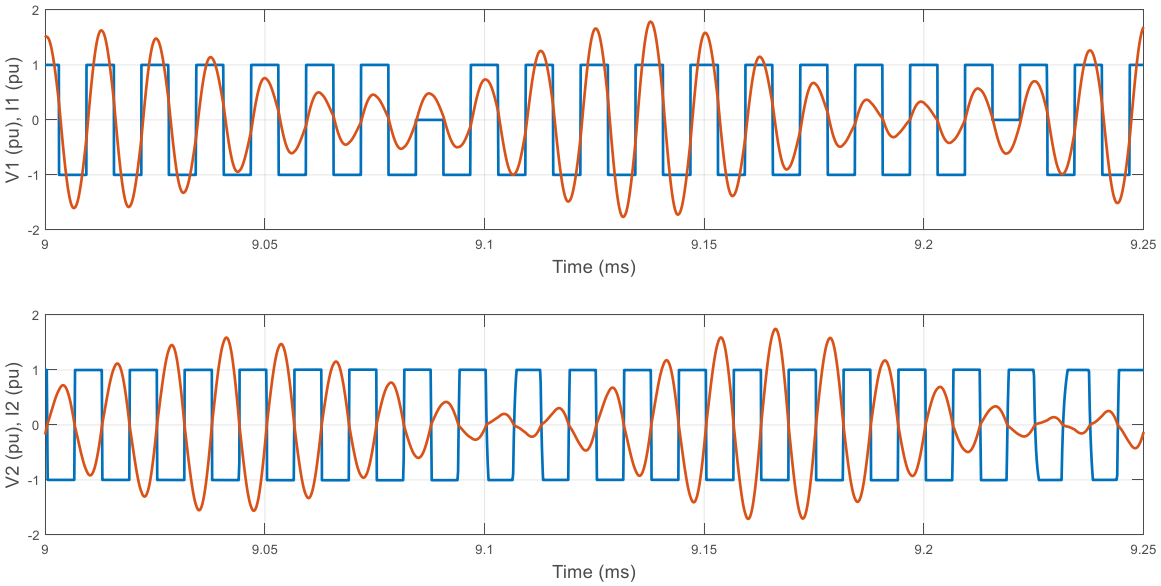

(a) – Conventional 1-bit Sigma-Delta modulator

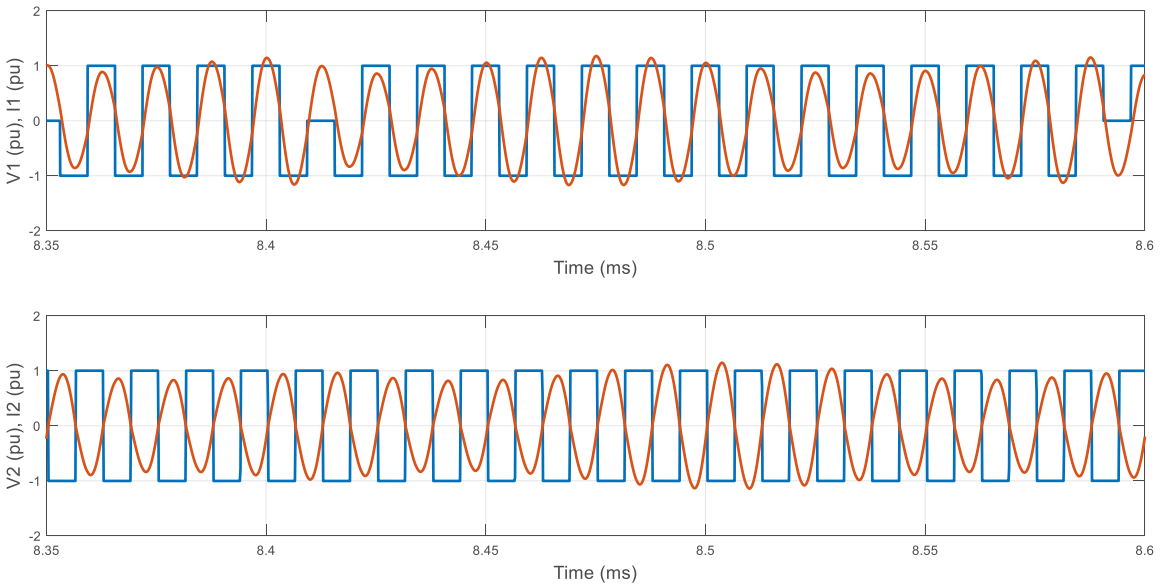

(b) – Modified, Conditional Sigma-Delta modulation

Fig. 8: Simulated voltage and current waveforms of 100 kW IPT system. Power reference set to 95% of rated.

randomization of the pulse-skipping process, thus avoiding limit cycles and persistent excitation of natural system modes. Effectiveness of the method can be seen in the simulation of Fig. 8 (b), which corresponds to the same operating conditions as in Fig. 8 (a). Suppression of the oscillations clearly reduces system losses, as seen from the last two columns in Table 2, and avoids the need for over-sizing of components.

5. CONCLUSION

Pulse-skipping voltage control methods are essential to achieve high efficiency operation of IPT systems. This aspect is particularly important for high power IPT systems designed to operate at high frequency, which is often the case when power density is a concern. The main issue with pulse-skipping methods is related to the possible appearance of poorly damped sub-harmonic oscillations that may result in high losses and in excessive values of current in the converter and/or excessive resonant voltage over the capacitors. This paper has clarified the cause of such oscillations and has shown that one of the most widely used algorithms, namely 1-bit DSM methods are prone to exciting the dominant undamped mode of the SS-compensated IPT

system for battery charging which exhibit CVL characteristics. A modification to the DSM implementation is presented, which avoids the insurgence of large current oscillations while retaining all the advantages of the original methos in terms of reduced switching losses.

REFERENCES

(1) A. Ahmad, M. S. Alam and R. Chabaan, “A Comprehensive Review of Wireless Charging Technologies for Electric Vehicles,” *IEEE Transactions on Transportation Electrification*, Vol. 4, No. 1, pp. 38-63, March 2018.

(2) C. R. Teeneti, T. T. Truscott, D. N. Beal and Z. Pantic, “Review of Wireless Charging Systems for Autonomous Underwater Vehicles,” *IEEE Journal of Oceanic Engineering*, vol. 46, no. 1, pp. 68-87, Jan. 2021.

(3) G. Guidi, J. A. Suul, F. Jenset, and I. Sorfonn, “Wireless charging for ships: high-power inductive charging for battery electric and plug-in hybrid vessels,” *IEEE Electrification Magazine*, vol. 5, no. 3, pp. 22–32, 2017.

(4) G. Guidi and J. A. Suul, “Minimizing converter requirements of inductive power transfer systems with constant voltage load and variable coupling conditions,” *IEEE Trans. Ind. Electron*, vol. 63, no. 11, pp. 6835–6844, Nov 2016.

(5) J. Zhou, G. Guidi and J. A. Suul, "Impact on Efficiency of Inductive Battery Charging System by Sub-Resonant Frequency Control during Large Variations in Coupling Conditions," in *Proceedings of the IEEE 21st Workshop on Control and Modeling for Power Electronics, COMPEL 2020*, Aalborg, Denmark, 2020

(6) J. Zhou, S. Chen, G. Guidi, Y. Tang and J. A. Suul, "Dynamic Improvement of Sub-Resonant Frequency Control for Inductive Power Transfer Systems by Coupling Estimation and Sending-Side Gain-Scheduled Control," in *IEEE Transactions on Industry Applications*, Vol. 60, No. 2, March/April 2024, pp. 3734-3745

(7) J. Zhou, G. Guidi, J. A. Suul, “Coordinated Voltage-Frequency Control for High-Efficiency Full-Range Operation of Inductive Battery Charging Systems with Large Coupling Variations,” accepted for publication in the *IEEE Journal of Emerging and Selected Topics in Power Electronics*, December 2024

(8) G. Guidi, J. A. Suul, " Modelling techniques for designing high-performance on-road dynamic charging systems for electric vehicles," in *Proceedings of the 31st International Electric Vehicle Symposium and Exhibition & International Electric Vehicle Technology Conference*, EVS31 & EVTeC 2018, Kobe, Japan, 30 September – 3 October 2018, 7 pp.

(9) J. Zhou, G. Guidi, K. Ljøkelsøy and J. A. Suul, "Evaluation and Suppression of Oscillations in Inductive Power Transfer Systems With Constant Voltage Load and Pulse Skipping Modulation," in *IEEE Transactions on Power Electronics*, vol. 38, no. 8, pp. 10412-10425, Aug. 2023.

(10) J. Zhou, G. Guidi, S. Chen, Y. Tang and J. A. Suul, "Conditional Pulse Density Modulation for Inductive Power Transfer Systems," in *IEEE Transactions on Power Electronics*, vol. 39, no. 1, pp. 88-93.

(11) J. Zhou, G. Guidi, S. Chen, Y. Tang, J. A. Suul, "A Hysteresis ON-OFF Control Method of Inductive Power Transfer Systems with Low Output Ripples and Fast Transient Responses," in *Proceedings of the 48th Annual Conference of the IEEE Industrial Electronics Society*, IECON 2022, Brussels, Belgium, 17-20 October 2022, 7 pp.

(12) Z. Karami, G. Guidi and J. A. Suul, "Finite-Control-Set Model Predictive Control to Suppress Oscillations in Inductive Power Transfer Systems with Constant Voltage Load," in *Proceedings of the 49th Annual Conference of the IEEE Industrial Electronics Society*, IECON 2023, Singapore, 16-19 October 2023, 7 pp.

(13) S. R. Sanders, J. M. Noworolski, X. Z. Liu, G. C. Verghese, "Generalized Averaging Method for Power Conversion Circuits," in *IEEE Transactions on Power Electronics*, Vol. 6, No. 2, pp. 251-259, April 1991

(14) H. Li, J. Fang, and Y. Tang, “Dynamic phasor-based reduced-order models of wireless power transfer systems,” in *IEEE Transactions on Power Electronics*, vol. 34, no. 11, pp. 11361–11370, Nov. 2019.

(15) S. Tian, F. C. Lee, and Q. Li, “A simplified equivalent circuit model of series resonant converter,” in *IEEE Transactions on Power Electronics*, vol. 31, no. 5, pp. 3922–3931, May 2016.

(16) J. Zhou, X. Wang, C. Q. Jiang, Y. Fan, T. Ma and J. Xiang, "Coupling Coefficient Estimation in Inductive Power Transfer Systems Through Damped Frequency," in *IEEE Transactions on Power Electronics*, vol. 39, no. 10, pp. 11991-11996, Oct. 2024

(17) S. Li and C. C. Mi, “Wireless power transfer for electric vehicle applications,” *IEEE Journal of Emerging and Selected Topics in Power Electronics*, vol. 3, no. 1, pp. 4–17, Mar. 2015.

(18) G. Guidi, J.A. Suul, “High Power and Power Density Inductive Charging System for Busses and Heavy-duty Vehicles,” in *Proceedings of the 6th International Electric Vehicle Technology Conference*, EVTeC 2023, Yokohama, Japan, 22-24 May 2023, 8 pp.

(19) Infineon-FF2MR12KM1-DataSheet-v02_00-EN. Downloaded from www.infineon.com.

(20) W. Zhong and S. Y. R. Hui, "Maximum energy efficiency operation of series-series resonant wireless power transfer systems using on-off keying modulation", in *IEEE Transactions on Power Electronics*, vol. 33, no. 4, pp. 3595-3603, Apr. 2018.

(21) Y. Li et al., "Enhanced On-Off Keying Modulation for Wireless Power Transfer Systems to Improve Efficiency Over a Wide Load Range," in *IEEE Transactions on Vehicular Technology*, vol. 73, no. 5, pp. 6409-6419, May 2024.

(22) V. Esteve et al., “Improving the efficiency of IGBT series-resonant inverters using pulse density modulation,” in *IEEE Transactions on Industrial Electronics*, vol. 58, no. 3, pp. 979–987, Mar. 2011.

(23) V. Esteve et al., “Enhanced pulse-density-modulated power control for high-frequency induction heating inverters,” *IEEE Transactions on Industrial Electronics*, vol. 62, no. 11, pp. 6905–6914, Nov. 2015.